

Synthesis of palladium–carbon nanotube–metal organic framework composite and its application as electrocatalyst for hydrogen production

Zahra Ghiamaty¹ · Ali Ghaffarinejad^{1,2} · Mojtaba Faryadras³ · Abbas Abdolmaleki⁴ · Hojjat Kazemi⁵

Received: 4 June 2016 / Accepted: 5 August 2016 / Published online: 11 August 2016
© The Author(s) 2016. This article is published with open access at Springerlink.com

Abstract There are very rare reports on using metal–organic framework (MOF) catalysts for electrochemical hydrogen production. In this study, a composite of palladium, single-walled carbon nanotube (SWCNT) and MOF-199 (Pd/SWCNTs@MOF-199) was synthesized by hydrothermal method, and its application as electrocatalyst in carbon paste electrode (CPE) structure for hydrogen production was studied. Scanning electron microscopy, X-ray diffraction, Brunauer–Emmett–Teller and thermal gravimetric analysis were used to characterize Pd/SWCNTs@MOF-199 catalyst. The performance of the proposed modified CPE for electrochemical hydrogen production was studied by cyclic voltammetry, linear sweep voltammetry, electrochemical impedance spectroscopy and chronoamperometry techniques. The effect of solution pH and the amount of binder and catalyst in the paste composition were investigated. The results showed

that the CPE modified with Pd/SWCNTs@MOF-199 reveals better catalytic characteristics such as highest catalytic activity and lowest onset potential compared to CPE and CPE modified with MOF-199 for hydrogen production in aqueous solution.

Keywords Metal organic framework composite · Electrochemical hydrogen production · Carbon paste electrode · Electrocatalyst

Introduction

Today, fossil fuels with disadvantages such as limited resources, warming up the earth and the environmental pollution are known as the main energy sources. Many efforts are being made to use other energy sources instead of fossil fuels which do not have disadvantages mentioned above. Nuclear energy, which its sources are limited, and working with it requires training of skilled manpower and use of advanced systems for protection against radioactive waste, will not be able to supply the required energy of the world.

Nowadays, hydrogen as a raw material is used in different industries [1]. Hydrogen produces high amount of energy with almost no pollution. It is a renewable energy carrier, and its resource is infinite [2]. An energy carrier can change energy to the forms which are usable to consumers. Although, renewable energy sources such as sun and wind cannot provide energy all the time, they could produce electric energy and hydrogen, which can be stored and transported until they are needed.

Several ways such as hydrolysis [3], thermal catalysis and thermochemical [4, 5], photocatalysis [6, 7], photoelectrocatalysis [8], steam reforming [9], gasification [10]

Electronic supplementary material The online version of this article (doi:10.1007/s40097-016-0203-4) contains supplementary material, which is available to authorized users.

✉ Ali Ghaffarinejad
Ghaffarinejad@iust.ac.ir

¹ Research Laboratory of Real Samples Analysis, Faculty of Chemistry, Iran University of Science and Technology, Tehran 1684613114, Iran

² Electroanalytical Chemistry Research Centre, Iran University of Science and Technology, Tehran 1684613114, Iran

³ Faculty of Chemistry, Iran University of Science and Technology, Tehran 1684613114, Iran

⁴ Department of Chemistry, Malek-Ashtar University of Technology, Tehran, P.O. Box 16765-34543, Iran

⁵ Research Institute of Petroleum Industry, Tehran 1485733111, Iran

and electrolysis [5, 11] are used to produce hydrogen. Although in the electrochemical studies platinum (Pt) is known as an excellent electrode for hydrogen generation, but because of limitation of its resource and its expensive price we should look for a suitable alternative to Pt [12]. There are several reports which have attempted to reduce the amount of loaded Pt in the electrode body [13] or replace it with another catalyst [14–16].

MOFs are synthesis by linking inorganic and organic units by strong bonds that lead to combined properties of organic and inorganic porous materials [17–19]. Among the wide range of available catalysts, MOFs have recently received noticeable attention owing to their characteristics such as porosity, specific surface area and adjustable pore size [20, 21]. Related to hydrogen energy, MOFs have been mostly used for hydrogen storage [22–25] and there are some reports in hydrogen generation area with photocatalytic method [26–28], and a few reports for electrochemical hydrogen generation [29–31].

In this study, a composite of MOF-199 with Pd and single-walled carbon nanotube (SWCNT) was prepared (Pd/SWCNTs@ MOF-199), and was applied for electrochemical hydrogen generation. Structure and morphology of the composite were characterized by various techniques, and its electrochemical hydrogen generation performance was compared with MOF-199 in CPE.

Experimental

Apparatus and software

The electrochemical impedance measurements were performed with an Autolab potentiostat/galvanostat (PGSTAT30) equipped with FRA board, also all other electrochemical studies were done with a μ -Autolab type II potentiostat/galvanostat that the software for both of them was Nova version 1.7.8. A three electrode cell containing, Pt rod as the counter electrode, bare or modified CPE as working electrode and Ag/AgCl (3 M KCl) as the reference electrode was used. In this paper, for easier comparison with other reports all potential values are reported vs. reversible hydrogen electrode (RHE). Teflon cylinder (3.0 mm i.d.) that was firmly packed with carbon paste was used as the body of the working electrode. To creation electrical connect a stainless steel rod inserted into the carbon paste. All electrochemical experiments were done at room temperature, also before every experiment the electrolyte solution was deaerated with high purity nitrogen gas for at least 10 min.

The MOF structure was investigated between $5^\circ \leq 2\theta \leq 90^\circ$ with X-ray diffraction (XRD) instrument

model of PHILIPS 1830 with a Cu ($K\alpha$) radiation source ($\lambda = 1.5418 \text{ \AA}$).

The catalyst morphology and its elemental analysis was investigated with a scanning electron microscopy (SEM) (VEGA\TESCAN-XMU) equipped with energy dispersive X-ray analysis (EDX).

Thermogravimetric analysis (TGA) was used to determine the thermal behaviour of MOF-199 and Pd/SWCNT@MOF-199 using SHIMADZU, TG-50/DTA-50. The measurements were conducted at $10^\circ \text{C min}^{-1}$ from room temperature.

Nitrogen adsorption–desorption isotherms were measured at 77 K by a BET instrument model of ASAPTM micromeritics 2020.

Materials and solutions

Graphite fine powder (extra pure with P.S. <50 μm), paraffin oil (spectroscopic grade, Uvasol[®]), H_3PO_4 (85 %), KCl (99.5 %), H_2SO_4 (98 %), $\text{Cu}(\text{NO}_3)_2 \cdot 3\text{H}_2\text{O}$ (99.5 %), benzene-1,3,5-tricarboxylic acid (H_3BTC , 95 %), PdCl_2 (59 % Pd basis) and ethanol (96 %) were obtained from Merck and were used without further purifications. The single walled carbon nanotube (>95 %) was purchased from Sigma and was treated with nitric acid (5 M) for 15 min. After treatment, the SWCNTs were filtered and washed with deionised water to remove any remained nitric acid and impurities. All aqueous solutions were prepared with deionized water.

MOF-199 synthesis

MOF-199 was synthesized as previously reported [32]. In brief, 2.3268 g of $\text{Cu}(\text{NO}_3)_2 \cdot 3\text{H}_2\text{O}$ was dissolved in 24 mL deionized water, and 1.4140 g H_3BTC was dissolved in 24 mL ethanol. Both solutions were mixed with magnetic stirrer and then put into a 100 mL stainless steel autoclave at 120°C for 12 h. The product was washed with ethanol and water, and then put at 70°C for 30 min, and after this the resultant was put at 150°C for 30 min. The final product was MOF-199.

Pd/SWCNT synthesis

PdCl_2 (0.16 g) was dissolved in 5 mL ethanol, 0.10 g of treated SWCNT was added to the proposed solution, and was dispersed using ultrasonic bath. After dispersion, during stirring of the mixture, 1 mL hydrazine was added dropwise under nitrogen atmosphere. Then the pH was adjusted to 9 with 1 M NaOH solution. For complete reduction of palladium the mixture was stirred on the magnetic stirrer for 2 h at 100°C . Finally, the precipitate



was filtered and washed with deionized water and then dried in oven at 100 °C for 4 h. This product is called Pd/SWCNT.

Synthesis of Pd/SWCNTs@ MOF-199 nanocomposite

Pd/SWCNTs@MOF-199 nanocomposite was prepared according to a previously reported procedure for synthesis of SWCNT@MOF-5 [33]. For this purpose, 2.320 g of $\text{Cu}(\text{NO}_3)_2 \cdot 3\text{H}_2\text{O}$ was dissolved in 24 mL deionized water, and 1.414 g H_3BTC was dissolved in 24 mL ethanol. Both solutions were mixed with magnetic stirrer for 20 min. Then 0.100 g of Pd/SWCNTs was added to the obtained solution, and was stirred for about 24 h at room temperature. The resultant mixture was transferred to autoclave and heated at 120 °C for 12 h. The precipitate was filtered, and washed with boiling deionized water and acetone. The washed precipitate was dried in vacuum oven at 100 °C for 4 h. The final product (Pd/SWCNTs@MOF-199 nanocomposite) was characterized with BET, TGA, XRD, EDX and SEM.

Preparation of bare and modified CPEs

Paraffin oil (as binder) and graphite powder (15:85 wt%) were mixed with an agate mortar to obtain a carbon paste. The modified carbon pastes were obtained by mixing a certain amount of Pd/SWCNTs@MOF-199 or MOF-199 (as modifiers) with binder and graphite. For preparation of the bare and modified electrodes, the working electrode cavities with 3 mm diameter were filled with unmodified and modified pastes. For removing any holes and improve the conductivity the pastes were packed on a smooth surface. Before each electrochemical measurement the electrode surface was renewed, polished on a smooth weighing paper, and washed with deionized water.

Results and discussion

Morphological characterization of Pd/SWCNTs@MOF-199

Figure 1 shows the SEM images of the MOF-199 and Pd/SWCNT@MOF-199. Figure 1a shows that the synthesized MOF-199 has a regular octahedral structure. Figure 1b shows the MOF-199 after modification with Pd/SWCNT, in which the carbon nanotubes on the octahedral shaped MOF-199 is clearly observed.

For a more exact examination, the EDX analysis of Pd/SWCNT@MOF-199 was also performed. Figure 2 shows

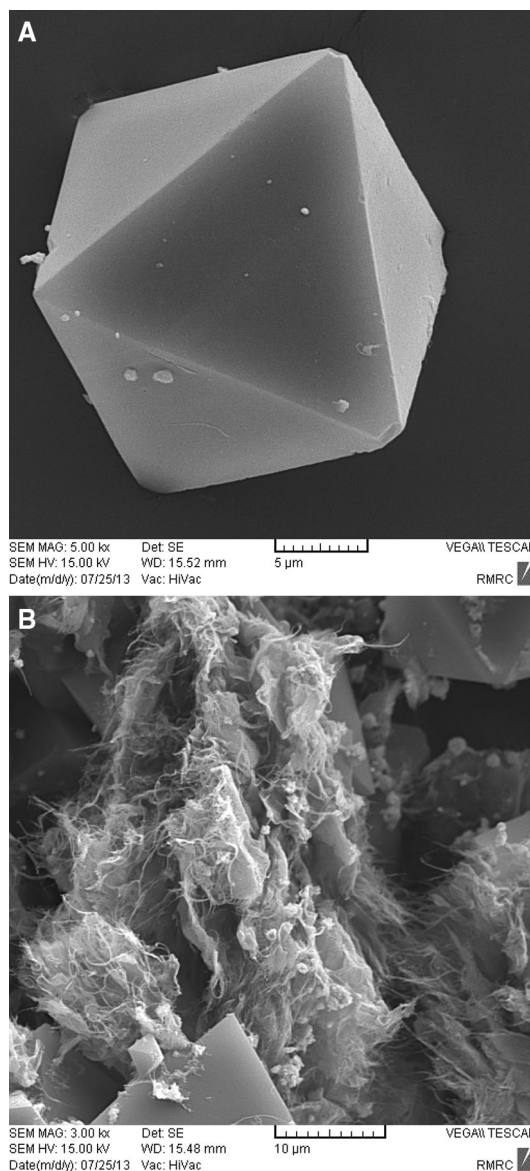
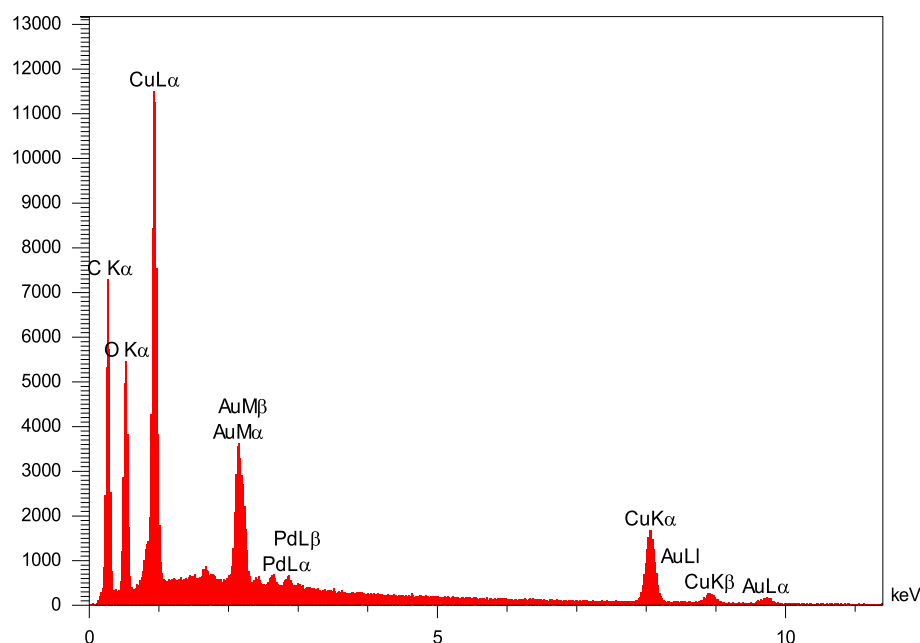


Fig. 1 SEM images of MOF-199 (a), and Pd/SWCNTs@MOF-199 nanocomposite (b)

the EDX analysis for Pd/SWCNT@MOF-199. In this experiment the presence of Cu and Pd is confirmed. As shown in this figure, the weak peaks observed in the EDX spectrum between 2 and 3 keV are related to Pd L_{α} and Pd L_{β} , which reveals the loaded Pd in the composite is low. In relation to EDX analysis data the Pd and Cu wt% are 17.62 and 0.98 %, respectively. According to the Pd:Cu mole ratio in the feed (about 1:27) and according to EDX analysis (about 1:30) it could be concluded that this ratio is almost constant after composite synthesis. The Au peaks are related to gold coating for the sample preparation before taking SEM images and it is not an impurity in the composite.

Fig. 2 EDX analysis of the Pd/SWCNTs@MOF-199 nanocomposite



X-ray diffraction (XRD) characterization of nanocomposite

The X-ray diffraction pattern of the MOF-199 is illustrated in Fig. 3A. The peaks between 10° and 20° are related to cubic crystalline structure of MOF-199, which is consistent with previous reports [34]. The peaks at 37° and 43° are related to Cu_2O impurities, but their intensities are very low related to main peaks of the MOF-199, which confirm that the purity of the MOF is reasonable. Figure 3B shows the XRD pattern of the Pd/SWCNT@MOF-199. In this pattern the main peak of $\text{Cu}_3(\text{BTC})_2$ at 11.68° corresponds to plane (2 2 2) reflection is not changed after modification, which indicates that the crystal structure of MOF-199 after modification has not changed. The peaks at 40.2° and 46.5° with the relative intensity of 10–15 % are related to the reflection of cubic unit cells of Pd.

Thermogravimetric analysis

Thermal stability of MOF-199 in the air atmosphere was analysed with thermal gravimetric analysis (TGA). Figure 4a illustrates that this compound is stable up to 300°C . The weight loss is observed in two stages. The first stage ($25\text{--}240^\circ\text{C}$) is related to removal of water molecules from pores, and the solvent molecules trapped in the MOF structure during synthesis. In this stage a 22.15 % weight loss was observed. At the second stage degradation of OH groups and portion of organic frameworks at $300\text{--}350^\circ\text{C}$ occurred, which is responsible for a 46.50 % weight loss. Copper oxides are probably the final remaining products at higher temperatures. Figure 4b shows the TGA diagram for the Pd/SWCNT@MOF-199. As

illustrated in this figure the thermal stability of the composite is slightly better than MOF-199, which may be due to the presence of hydrophobic carbon nanotubes in its structure.

Determination of nitrogen adsorption–desorption isotherms

Figure 5a shows the N_2 adsorption–desorption isotherm of MOF-199, which according to IUPAC classification corresponds to type I isotherm. This isotherm indicates that the available porosity is in micrometer dimensions. Achieving to level off conditions and saturation at relatively low pressures emphasizes that the sample is microporous. At partial pressures near 1 atm some increase in adsorption is observed, which is related to accumulation of the existing porosities in the framework at relatively high pressures. Initial filling of porosities at low pressures in logarithmic scales represents that the porosities are small and there is an effective interaction between MOF and N_2 . In addition, negligible hysteresis loop in adsorption/desorption isotherm shows that most of holes are in the microporous range.

Figure 5b shows the N_2 adsorption–desorption isotherm of Pd/SWCNT@MOF-199. Results show that MOF modification with Pd does not change the microporous structure of MOF, but as expected the surface area is slightly decreased. Table 1 summarizes the results of these experiments.

Electrochemical hydrogen evolution reaction on Pd/SWCNTs@MOF-199 modified CPE

Electrochemical studies showed that Pd/SWCNTs@MOF-199 is a good electrocatalyst for HER. Therefore, for

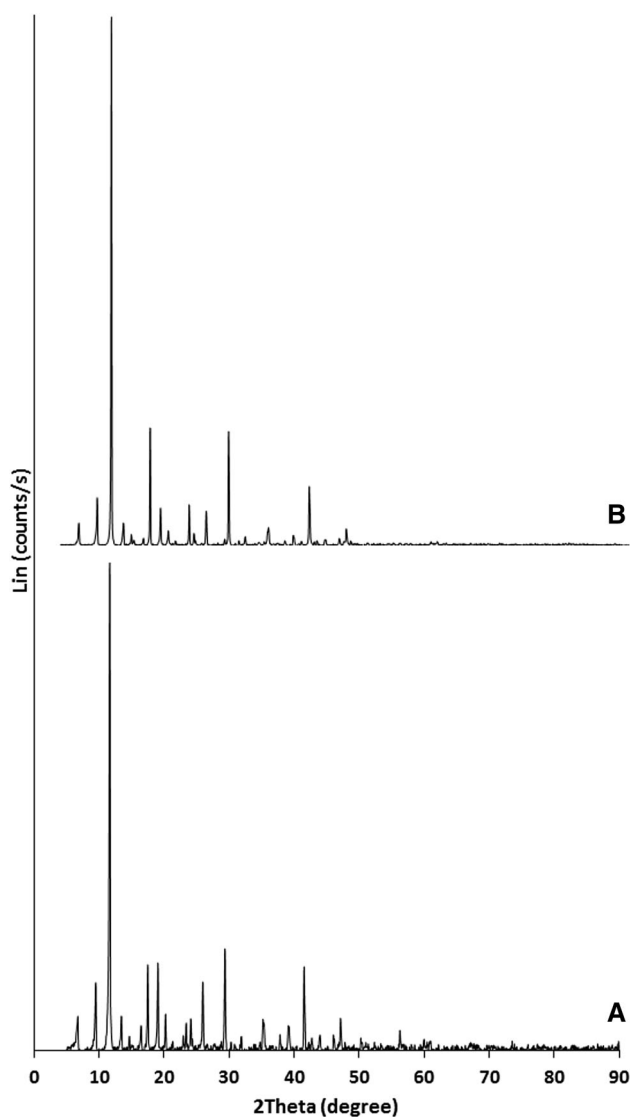


Fig. 3 XRD pattern of MOF-199 (A) and Pd/SWCNT@MOF-199 (B)

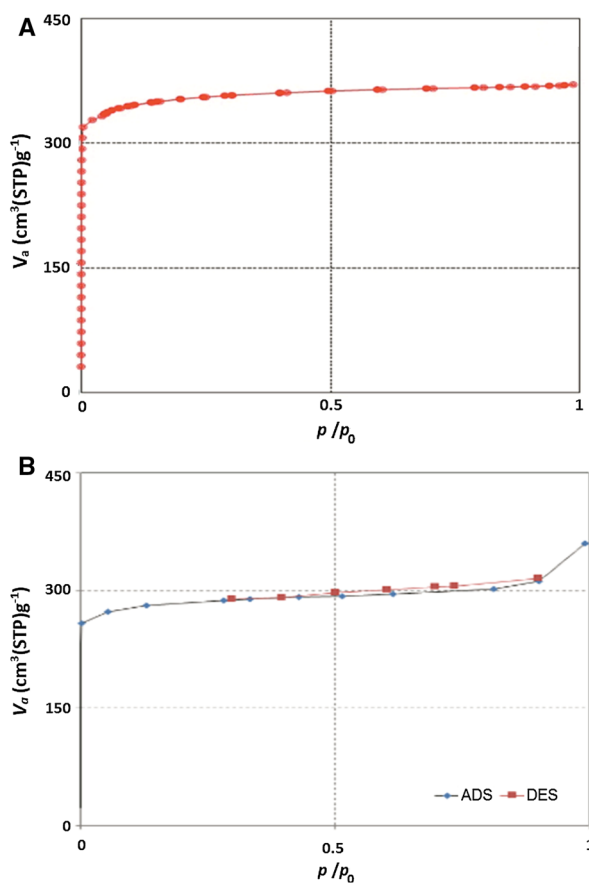
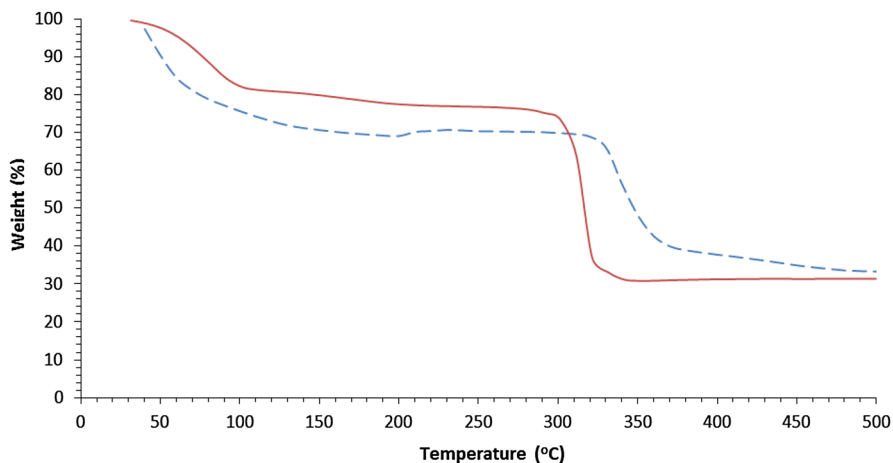


Fig. 5 Adsorption-desorption analysis at 77 K for MOF-199 (a), and Pd/SWCNT@MOF-199 (b)

Table 1 The structure data of the pores for MOF-199 and Pd/SWCNT@MOF-199 with adsorption-desorption analysis

Sample	V_p ($\text{cm}^3 \text{g}^{-1}$)	d spacing (nm)	A_{BET} ($\text{m}^2 \text{g}^{-1}$)
MOF-199	0.573	1.67	1370.0
Pd/SWCNTs@MOF-199	0.555	1.98	1125.8

Fig. 4 TGA thermograms of MOF-199 (solid line), and Pd/SWCNT@MOF-199 (dashed line)



further study, some important parameters including electrocatalyst amounts in the electrode composition, paraffin binder and electrolyte pH were optimized.

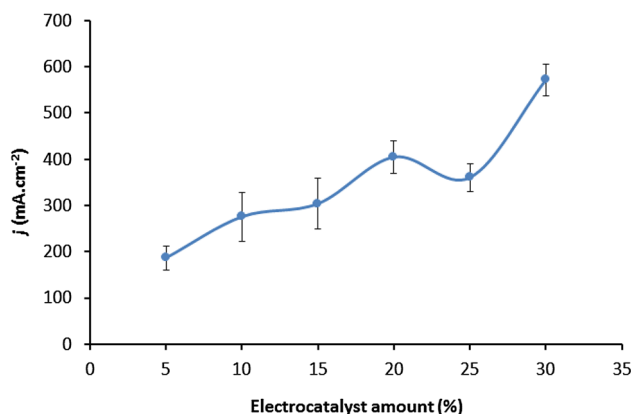


Fig. 6 The effect of catalyst amount on the HER performance. At each composition 20 successive CVs were applied and the j value at the last cycle was measured at -1 V (scan rate 100 mV s⁻¹, 15 % binder and 2 M sulphuric acid as supporting electrolyte, each point is the average of 3–5 measurements)

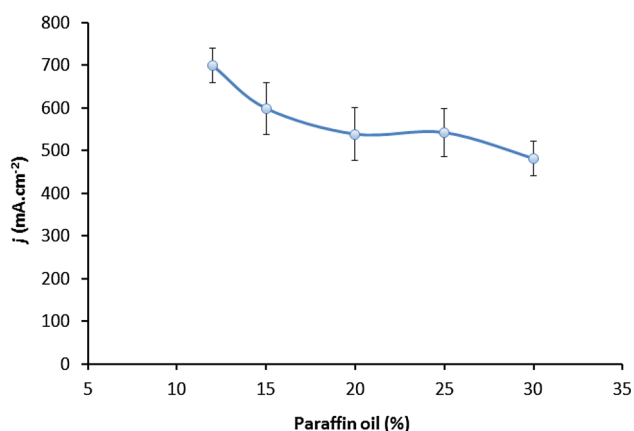
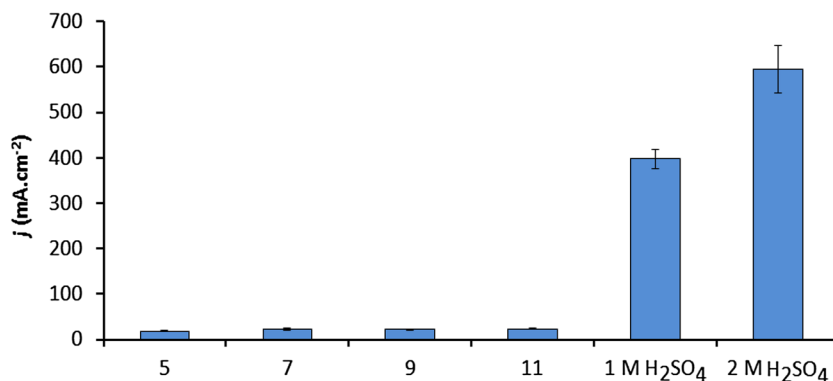


Fig. 7 The effect of oil binder amount on the HER performance. At each composition 20 successive CVs were applied and j at the last cycle was measured at -1 V (scan rate 100 mV s⁻¹, 30 % catalyst and 2 M sulphuric acid as supporting electrolyte, each point is the average of 3 or 5 measurements)

Fig. 8 The effect of supporting electrolyte pH on the HER performance for Pd/SWCNTs@MOF-199-CPE. At each solution 20 successive CVs were applied and j at the last cycle was measured at -1 V. (scan rate 100 mV s⁻¹, 30 % catalyst and 15 % Oil, each point is the average of 3 or 4 measurements)



The catalyst amount

For optimization of the catalyst amount, various percentages of Pd/SWCNTs@MOF-199 were added to the paste composition, while the paraffin percent was kept constant at 15 %. At these compositions 20 successive cyclic voltammograms (CVs) with the scan rate of 100 mV s⁻¹ at the potential range of 1.2 to -1 V were applied on the electrodes in 2 M sulphuric acid solution. At potential of -1 V the current density of the HER (j), which could be interpreted as the hydrogen production rate, was measured. The result of this study is summarized in Fig. 6. According to Fig. 6 it is obvious that the j value increasing is a direct consequence of increasing amount of catalyst. However, for catalyst amounts greater than 30 % the paste consolidation decreased, so 30 % was used for the rest of experiments.

Optimization of the paraffin binder amount

The conductivity and active surface area of the electrode can be affected by the amount of paraffin which is a non-conductive binder. According to this fact, the amount of binder was changed, while the catalyst percentage was kept at 30 % and the electrolyte was 2 M sulphuric acid, and the HER was investigated by applying 20 successive CVs on the electrode surface with the scan rate of 100 mV s⁻¹ in the potential range of 1.2 to -1 V. Figure 7 illustrates the plot of j at 1 V vs. paraffin oil percent under the mentioned conditions. Figure 7 clearly demonstrates that when the amount of binder is decreased, it favorably affected on the performance of the HER which can be related to the increase in electrode conductivity. Amounts lower than 12 % were not used, because at these compositions the paste consolidation was very poor.

pH effect

The effect of pH on HER efficiency on the Pd/SWCNTs@MOF-199-CPE was studied in 0.1 M

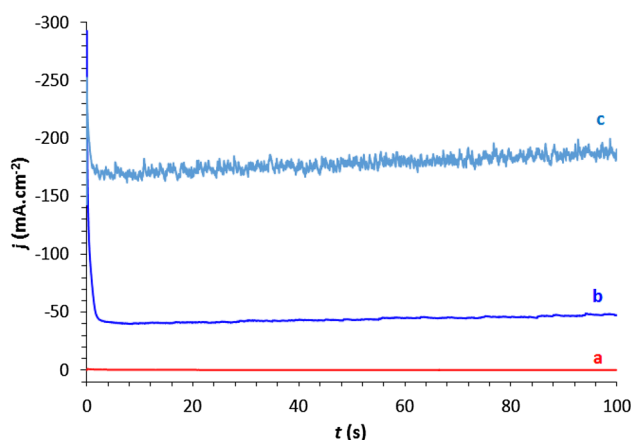


Fig. 9 Chronoamperometry on CPE (a), MOF-199-CPE (b) and Pd/SWCNTs@MOF-199-CPE (c) in 2 M H_2SO_4 with -0.6 V applied potential

phosphate buffer (pH = 5, 7, 9 and 11) and 1 and 2 M sulphuric acid solutions. The results of these experiments are illustrated in Fig. 8. By increasing the hydronium concentration, the current of hydrogen production increases, therefore, in this study the largest j was observed in 2 M sulphuric acid solution, so this solution was selected for the rest of experiments. More concentrated sulphuric acid, or other types of strong acids such as HNO_3 and HCl were not used because of their corrosive effects.

Chronoamperometry study

The electrode response stability was evaluated with chronoamperometry technique. In this experiment a constant potential (-0.6 V) was applied on CPE, MOF-199-CPE and Pd/SWCNTs@MOF-199-CPE under optimal conditions (Fig. 9). According to this figure the highest j for HER is observed for Pd/SWCNTs@MOF-199-CPE. Also the results of modified electrodes show that j does not decrease, but increases with time, and compare to CPE the current densities of HER on modified electrodes are considerably greater.

EIS studies

In this study before and after applying 20 successive CVs on the CPE, MOF-199-CPE and Pd/SWCNTs@MOF-199-CPE, the EIS test was done in 2 M H_2SO_4 in the frequency range of 5×10^{-2} to 1×10^5 Hz and at -0.25 V DC potential. Figure 10 shows that after applying CVs the wave height in the Bode plots, which is related to charge transfer resistance (R_{ct}), decreases. This observation confirms that successive CVs improve the rate of electron transfer. This improvement may be due to the activation of SWCNT and graphite surface.

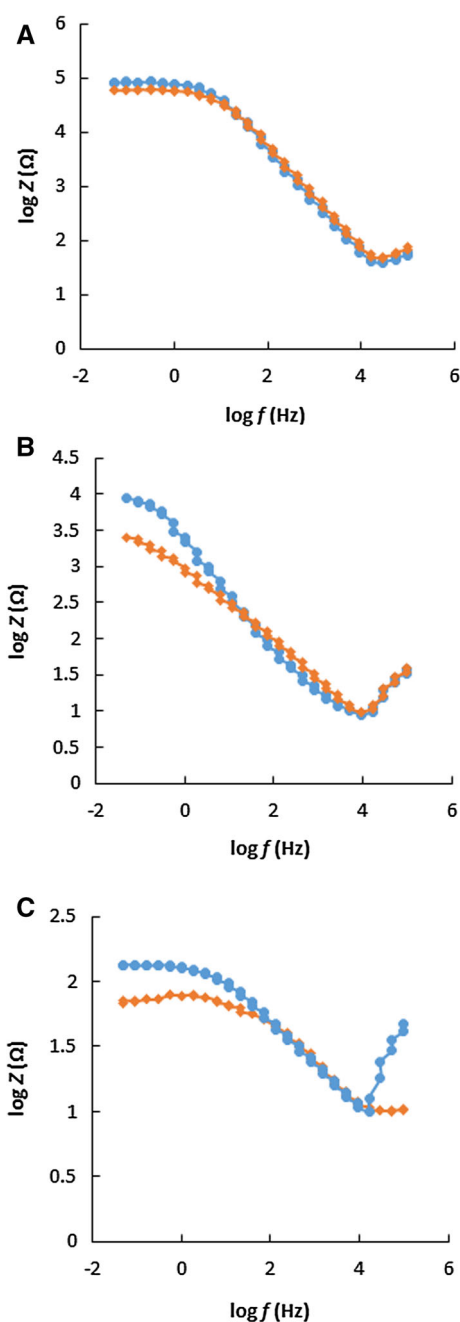


Fig. 10 Bode plots in 0.1 M KCl containing 10 mM $\text{K}_3\text{Fe}(\text{CN})_6$ in the frequency range of 5×10^{-2} to 1×10^5 Hz before (a) and after (b) applying 20 successive CVs in the HER process for CPE (a), MOF-199-CPE (b), and Pd/SWCNTs@MOF-199-CPE (c)

Steady-state polarization curves for HER at bare and modified CPEs

To evaluate electrocatalytic activities of CPE and modified CPEs, steady-state polarization curves for HER at electrodes were measured by linear sweep voltammetry (LSV) at a very low scan rate (1 mV s^{-1}) (Fig. 11). There is a

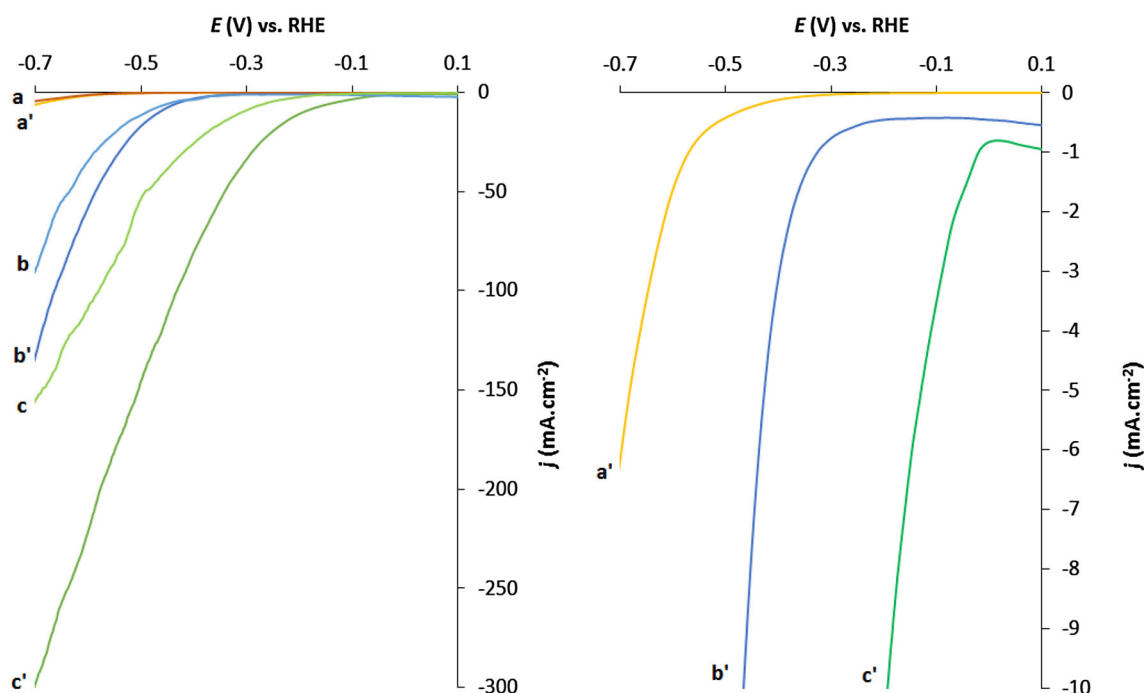


Fig. 11 LSV on CPE (a, a'), MOF-199-CPE (b, b') and Pd/SWCNTs@MOF-199-CPE (c, c') in 2 M H₂SO₄ with the scan rate of 1 mV s⁻¹ before and after (') applying 20 successive CVs in 2 M

H₂SO₄. The right panel is the magnification of the LSVs after applying CVs for better vision of the HER onset potential

Table 2 Tafel slopes (*b*), exchange current densities (*j*_o) and transfer coefficients (*α*) for HER at CPE, MOF-199-CPE and Pd/SWCNTs@MOF-199-CPE

Electrode	<i>b</i> (mV decade ⁻¹)		<i>j</i> _o (mA cm ⁻²)		<i>α</i>	
	Before	After	Before	After	Before	After
CPE	147	185	6.41 × 10 ⁻⁶	6.09 × 10 ⁻⁵	0.40	0.32
MOF-199-CPE	135	164	9.48 × 10 ⁻⁵	5.89 × 10 ⁻⁴	0.36	0.44
Pd/SWCNTs@ MOF-199-CPE	172	208	9.73 × 10 ⁻³	1.19 × 10 ⁻¹	0.34	0.28

linear relation between η and $\log j$ under steady-state condition and large cathodic overpotential (η), (Tafel equation),

$$\eta = \frac{2.3RT}{\alpha F} \log j_o - \frac{2.3RT}{\alpha F} \log j \text{ (Tafel equation),}$$

where R is the ideal gas constant (8.314 J mol⁻¹ K⁻¹), j_o is the exchange current density, T is the absolute temperature and F is the Faraday constant. For these three electrodes the values of Tafel slope (b), j_o and transfer coefficient (α) are summarized in Table 2.

The value of j_o increases for all three electrodes after applying CVs, which confirms again that the applied CVs improve the electron transfer rate (or decreases R_{ct}). The j_o values are in this order: Pd/SWCNTs@MOF-199-CPE > MOF-199-CPE > CPE. In right panel of the Fig. 11, the LSVs after applying CVs are magnified. According to these LSVs it is obvious that the lowest onset potential is for Pd/SWCNTs@MOF-199-CPE (about 0 V vs. RHE).

The results obtained from polarization and EIS studies both showed that the Pd/SWCNTs@MOF-199-CPE has the best performance related to CPE and MOF-199-CPE. The reason of this observation may be related to the presence of Pd and SWCNT in the composite structure. There are several reports which have used Pd as a catalyst for electrochemical hydrogen production [35, 36], but this metal is expensive, therefore, in this work the loaded Pd on the catalyst is low. Also there are some reports which have used carbon nanotubes in the electrode composition for electrochemical HER [37–39]. In addition, there are several reports which have applied the MOF [22–25], Pd [40, 41] and SWCNT [37, 38] as adsorbent for hydrogen, and one of the famous mechanisms for electrochemical HER in acidic media is based on hydrogen adsorption on the electrode surface in the rate determining step (Volmer reaction) [42]. Therefore, these materials by improving hydrogen adsorption can facilitate the HER progress.

In comparison with the first report for electrochemical HER with polyoxometalate-based metal organic



frameworks (POMOFs) [29], although the onset potential is relatively higher, but it seems that the j value for the proposed electrode is greater. Also compared to two recently published reports for electrochemical HER on MOF-5 modified CPE [31] and Ni-based MOF modified GCE [30], the proposed modified CPE electrode has better current densities or onset potential for HER.

Conclusion

In this study, a nanocomposite of MOF-199 with SWCNT and Pd was synthesized and its characteristics was evaluated by XRD, BET, TGA and SEM. According to the rare reports for application of MOFs in electrochemical hydrogen generation, the performance of this composite as an electrocatalyst in CPE was studied, and some important parameters were optimized. The results show that this modifier has a good performance for HER, which compared to MOF-199 and bare CPE has the best performance. Also electrochemical studies showed that applying successive CVs or a constant potential on the electrodes surface does not decrease the electrode performance, but improves the electrocatalytic properties.

Acknowledgments We gratefully acknowledge the partial support of this work from the Research Council of the Iran University of Science and Technology.

Open Access This article is distributed under the terms of the Creative Commons Attribution 4.0 International License (<http://creativecommons.org/licenses/by/4.0/>), which permits unrestricted use, distribution, and reproduction in any medium, provided you give appropriate credit to the original author(s) and the source, provide a link to the Creative Commons license, and indicate if changes were made.

References

- Dincer, I.: Environmental and sustainability aspects of hydrogen and fuel cell systems. *Int. J. Energy Res.* **31**, 29–55 (2007)
- Momirlan, M., Veziroglu, T.N.: The properties of hydrogen as fuel tomorrow in sustainable energy system for a cleaner planet. *Int. J. Hydrogen Energy* **30**, 795–802 (2005)
- Liu, B., Li, Z.: A review: hydrogen generation from borohydride hydrolysis reaction. *J. Power Sources* **187**, 527–534 (2009)
- Naterer, G.F., Suppiah, S., Stolberg, L., Lewis, M., Wang, Z., Daggupati, V., Gabriel, K., Dincer, I., Rosen, M.A., Spekkens, P., Lvov, S.N., Fowler, M., Tremaine, P., Mostaghimi, J., Easton, E.B., Trevani, L., Rizvi, G., Ikeda, B.M., Kaye, M.H., Lu, L., Pioro, I., Smith, W.R., Secnik, E., Jiang, J., Avsec, J.: Canada's program on nuclear hydrogen production and the thermochemical Cu–Cl cycle. *Int. J. Hydrogen Energy* **35**, 10905–10926 (2010)
- Balta, M.T., Dincer, I., Hepbasli, A.: Geothermal-based hydrogen production using thermochemical and hybrid cycles: a review and analysis. *Int. J. Energy Res.* **34**, 757–775 (2010)
- Shen, S., Guo, L., Chen, X., Ren, F., Mao, S.S.: Effect of Ag₂S on solar-driven photocatalytic hydrogen evolution of nanostructured CdS. *Int. J. Hydrogen Energy* **35**, 7110–7115 (2010)
- Mangrulkar, P.A., Joshi, M.V., Kamble, S.P., Labhsetwar, N.K., Rayalu, S.S.: Hydrogen evolution by a low cost photocatalyst: bauxite residue. *Int. J. Hydrogen Energy* **35**, 10859–10866 (2010)
- Zhao, W., Wang, Z., Shen, X., Li, J., Xu, C., Gan, Z.: Hydrogen generation via photoelectrocatalytic water splitting using a tungsten trioxide catalyst under visible light irradiation. *Int. J. Hydrogen Energy* **37**, 908–915 (2012)
- Avasthi, K.S., Reddy, R.N., Patel, S.: Challenges in the production of hydrogen from glycerol—a biodiesel byproduct via steam reforming process. *J. Proc. Eng.* **51**, 423–429 (2013)
- Khan, Z., Yusup, S., Ahmad, M.M., Rashidi, N.A.: Integrated catalytic adsorption (ICA) steam gasification system for enhanced hydrogen production using palm kernel shell. *Int. J. Hydrogen Energy* **39**, 3286–3293 (2014)
- Wang, M., Wang, Z., Gong, X., Guo, Z.: The intensification technologies to water electrolysis for hydrogen production—a review. *Renew. Sustain. Energy Rev.* **29**, 573–588 (2014)
- Yang, J., Cheng, F., Liang, J., Chen, J.: Hydrogen generation by hydrolysis of ammonia borane with a nanoporous cobalt–tungsten–boron–phosphorus catalyst supported on Ni foam. *Int. J. Hydrogen Energy* **36**, 1411–1417 (2011)
- Raof, J.B., Ojani, R., Esfeden, S.A., Nadimi, S.R.: Fabrication of bimetallic Cu/Pt nanoparticles modified glassy carbon electrode and its catalytic activity toward hydrogen evolution reaction. *Int. J. Hydrogen Energy* **35**, 3937–3944 (2011)
- Ghaffarinejad, A., Sadeghi, N., Kazemi, H., Khajehzadeh, A., Amiri, M., Noori, A.: Effect of metal hexacyanoferrate films on hydrogen evolution reaction. *J. Electroanal. Chem.* **685**, 103–108 (2012)
- Ghaffarinejad, A., Magsoudi, E., Sadeghi, N.: Hydrogen generation by shimalite Ni catalyst. *Anal. Bioanal. Chem.* **5**, 316–324 (2013)
- Safavi, A., Kazemi, H., Kazemi, S.H.: In situ electrodeposition of graphene/nano-palladium on carbon cloth for electrooxidation of methanol in alkaline media. *J. Power Sources* **256**, 354–360 (2014)
- Klein, N., Senkovska, I., Gedrich, K., Stoeck, U., Henschel, A., Mueller, U., Kaskel, S.: A mesoporous metal–organic framework. *Angew. Chem. Int. Ed.* **48**, 9954–9957 (2009)
- O'Keeffe, M., Eddaoudi, M., Li, H., Reineke, T., Yaghi, O.M.: Frameworks for extended solids: geometrical design principles. *J. Solid State Chem.* **152**, 3–20 (2000)
- Hoskins, B., Robson, R.: Design and construction of a new class of scaffolding-like materials comprising infinite polymeric frameworks of 3D-linked molecular rods. A reappraisal of the zinc cyanide and cadmium cyanide structures and the synthesis and structure of the diamond-related frameworks [N(CH₃)₄][Cu^IZn^{II}(CN)₄] and Cu^I [4, 4', 4'', 4'''-tetracyanotetraphenylmethane]BF₄·xC₆H₅N. *J. Am. Chem. Soc.* **112**, 1546–1554 (1990)
- Oh, M., Mirkin, C.A.: Chemically tailorable colloidal particles from infinite coordination polymers. *Nature* **438**, 651–654 (2005)
- Lee, J., Farha, O.K., Roberts, J., Scheidt, K.A., Nguyen, S.T., Hupp, J.T.: Metal–organic framework materials as catalysts. *Chem. Soc. Rev.* **38**, 1450–1459 (2009)
- Rowell, J.L., Yaghi, O.M.: Strategies for hydrogen storage in metal–organic frameworks. *Angew. Chem. Int. Ed.* **44**, 4670–4679 (2005)
- Murray, L.J., Dincă, M., Long, J.R.: Hydrogen storage in metal–organic frameworks. *Chem. Soc. Rev.* **38**, 1294–1314 (2009)
- Moellmer, J., Moeller, A., Dreisbach, F., Glaeser, R., Staudt, R.: High pressure adsorption of hydrogen, nitrogen, carbon dioxide and methane on the metal–organic framework HKUST-1. *J. Microporous Mesoporous Mat.* **138**, 140–148 (2011)
- Lim, D.W., Chyun, S.A., Suh, M.P.: Hydrogen storage in a potassium-ion-bound metal-organic framework incorporating



- crown ether struts as specific cation binding sites. *Angew. Chem. Int. Ed.* **53**, 7819–7822 (2014)
26. Wen, M., Mori, K., Kamegawa, T., Yamashita, H.: Amine-functionalized MIL-101 (Cr) with imbedded platinum nanoparticles as a durable photocatalyst for hydrogen production from water. *Chem. Commun.* **50**, 11645–11648 (2014)
 27. Toyao, T., Saito, M., Dohshi, S., Mochizuki, K., Iwata, M., Higashimura, H., Horiuchi, Y., Matsuoka, M.: Development of a Ru complex-incorporated MOF photocatalyst for hydrogen production under visible-light irradiation. *Chem. Commun.* **50**, 6779–6781 (2014)
 28. He, J., Wang, J., Chen, Y., Zhang, J., Duan, D., Wang, Y., Yan, Z.: A dye-sensitized Pt@ UiO-66 (Zr) metal–organic framework for visible-light photocatalytic hydrogen production. *Chem. Commun.* **50**, 7063–7066 (2014)
 29. Nohra, B., El Moll, H., Rodriguez Albelo, L.M., Mialane, P., Marrot, J., Mellot-Draznieks, C., O’Keeffe, M., Ngo Biboum, R., Lemaire, J., Keita, B., Nadjo, L., Dolbecq, A.: Polyoxometalate-based metal organic frameworks (POMOFs): structural trends, energetics, and high electrocatalytic efficiency for hydrogen evolution reaction. *J. Am. Chem. Soc.* **133**, 13363–13374 (2011)
 30. Tian, T., Ai, L., Jiang, J.: Metal–organic framework-derived nickel phosphides as efficient electrocatalysts toward sustainable hydrogen generation from water splitting. *RSC Adv.* **5**, 10290–10295 (2015)
 31. Yang, H.M., Song, X.L., Yang, T.L., Liang, Z.H., Fan, C.M., Hao, X.G.: Electrochemical synthesis of flower shaped morphology MOFs in an ionic liquid system and their electrocatalytic application to the hydrogen evolution reaction. *RSC Adv.* **4**, 15720–15726 (2014)
 32. Xiang, Z., Cao, D., Shao, X., Wang, W., Zhang, J., Wu, W.: Facile preparation of high-capacity hydrogen storage metal–organic frameworks: a combination of microwave-assisted solvothermal synthesis and supercritical activation. *Chem. Eng. Sci.* **65**, 3140–3146 (2010)
 33. Yang, S.J., Choi, J.Y., Chae, H.K., Cho, J.H., Nahm, K.S., Park, C.R.: Preparation and enhanced hydrostability and hydrogen storage capacity of CNT@ MOF-5 hybrid composite. *Chem. Mater.* **21**, 1893–1897 (2009)
 34. Loera-Serna, S., Oliver-Tolentino, M.A., de Lourdes López-Núñez, M., Santana-Cruz, A., Guzmán-Vargas, A., Cabrera-Sierra, R., Beltrán, H.I., Flores, J.: Electrochemical behavior of [Cu₃(BTC)₂] metal–organic framework. The effect of the method of synthesis. *J. Alloy. Compd.* **540**, 113–120 (2012)
 35. Searson, P.C.: Hydrogen evolution and entry in palladium at high current density. *J. Acta Metal. Mater.* **39**, 2519–2525 (1991)
 36. Safavi, A., Kazemi, S.H., Kazemi, H.: Electrocatalytic behaviors of silver–palladium nanoalloys modified carbon ionic liquid electrode towards hydrogen evolution reaction. *J. Fuel* **118**, 156–162 (2014)
 37. Fernandez, P., Castro, E., Real, S., Martins, M.: Electrochemical behavior of single walled carbon nanotubes—hydrogen storage and hydrogen evolution reaction. *Int. J. Hydrogen Energy* **34**, 8115–8126 (2009)
 38. Prossini, P.P., Pozio, A., Botti, S., Ciardi, R.: Electrochemical studies of hydrogen evolution, storage and oxidation on carbon nanotube electrodes. *J. Power Sources* **118**, 265–269 (2013)
 39. Paunović, P., Dimitrov, A.T., Popovski, O., Slavcheva, E., Grozdanov, A., Lefterova, E., Petruševski, G., Jordanov, S.H.: Effect of activation/purification of multiwalled carbon nanotubes (MWCNTs) on the activity of non-platinum based hypo-hyper d-electrocatalysts for hydrogen evolution. *J. Mater. Res. Bull.* **44**, 1816–1821 (2009)
 40. Conrad, H., Ertl, G., Latta, E.E.: Adsorption of hydrogen on palladium single crystal surfaces. *Surf. Sci.* **41**, 435–446 (1974)
 41. Lopez, M.J., Cabria, I., Alonso, J.A.: Palladium clusters anchored on graphene vacancies and their effect on the reversible adsorption of hydrogen. *J. Phys. Chem. C* **118**, 5081–5090 (2014)
 42. Abbaspour, A., Mirahmadi, E.: Electrocatalytic hydrogen evolution reaction on carbon paste electrode modified with Ni ferrite nanoparticles. *J. Fuel* **104**, 575–582 (2013)

